TITLE PAGE

Altenusin, a non-steroidal microbial metabolite, attenuates non-alcoholic fatty liver disease by activating the farnesoid X receptor

Zhihui Zheng, Zanmei Zhao, Shuqiang Li, Xinhua Lu, Mengxi Jiang, Jie Lin, Yunqi An, Yang Xie, Meishu Xu, Wenbin Shen, Grace L. Guo, Yixian Huang, Song Li, Xuexia Zhang, Wen Xie

Center for Pharmacogenetics and Department of Pharmaceutical Sciences, University of Pittsburgh, Pittsburgh, PA 15261, USA (Z.Z., Z.Z., M.J., Y.A., Y.X., M.X., Y.H., S.L., W.X.).

New Drug Research & Development Center, North China Pharmaceutical Group Corporation, Shijiazhuang, Hebei 050015, China (Z.Z., X.L., J.L., W.S., X.Z.).

Occupational Disease Department, Peking University Third Hospital, Beijing 100191, China (Z.Z., S.L.).

Department of Pharmacology and Toxicology, School of Pharmacy, Rutgers University, Piscataway, NJ, USA (G.L.G.).

Department of Pharmacology & Chemical Biology, University of Pittsburgh, Pittsburgh, PA 15261, USA (W.X.).

1

Running title: A non-steroidal FXR agonist that inhibits NAFLD

Corresponding author:

Dr. Wen Xie, Center for Pharmacogenetics, 306 Salk Pavilion, University of

Pittsburgh, Pittsburgh, PA 15261, USA. E-mail: wex6@pitt.edu; or Dr. Xuexia Zhang,

New Drug Research & Development Center, North China Pharmaceutical Group

Corporation, Shijiazhuang, Hebei 050015, China. E-mail: zhangxuexiazxx@163.com.

Number of text pages: 38

Number of figures: 7

Number of table: 1

Number of references: 48

Number of words in the Abstract: 232

Number of words in Introduction: 604

Number of words in Discussion: 871

Abbreviations

ACC, acetyl-CoA carboxylase; ALT, alanine aminotransferase; aP2, adipocyte
protein 2; AST, aspartate aminotransferase; BSEP, bile salt export protein; CDCA,
chenodeoxycholic acid; CYP7A1, cholesterol-7α-hydroxylase; 6-ECDCA,
6α-ethyl-chenodeoxycholic acid; FAS, fatty acid synthase; FoxO1, forkhead box
protein O1; FXR, farnesoid X receptor; FXRE, FXR response element; G6Pase,
glucose-6-phosphatase; GSIS, glucose-stimulated insulin secretion; GTT, glucose
tolerance test; HFD, high-fat diet; ITT, insulin tolerance test; L-FABP, liver fatty
acid-binding protein; NAFLD, non-alcoholic fatty liver disease; PEPCK,
phosphoenolpyruvate carboxykinase; PPARγ, peroxisome proliferator-activated
receptor γ; SHP, small heterodimer partner; SR-B1, scavenger receptor class B1;
SREBP-1c, sterol-regulatory-element binding protein-1c; UCP, Uncoupling protein

Abstract

Non-alcoholic fatty liver disease (NAFLD) is a prevalent chronic liver disease. The incidence of NAFLD has increased steadily due to its close association with the global epidemic of obesity and type 2 diabetes. However, there is no effective pharmacological therapy approved for NAFLD. Farnesoid X receptor (FXR), a member of the nuclear receptor subfamily, plays important roles in maintaining the homeostasis of bile acids, glucose and lipids. FXR agonists have shown promise for the treatment of NAFLD. Here we report Altenusin (2076A), a natural non-steroidal fungal metabolite, as a novel selective agonist of FXR with an EC50 value of 3.2 ± 0.2 μM. Administration of 2076A protected mice from high-fat diet (HFD)-induced obesity by reducing the body weight and fat mass by 22.9% and 50.0%, respectively. Administration of 2076A also decreased the blood glucose level from 178.3 ± 12.4 mg/dL to 116.2 ± 4.1 mg/dL, the serum insulin level from 1.4 ± 0.6 ng/dL to 0.4 ± 0.1 ng/dL. Moreover, 2076A treatment nearly reversed HFD-induced hepatic lipid droplet accumulation and macrovescicular steatosis. These metabolic effects were abolished in FXR knockout mice. Mechanistically, the metabolic benefits of 2076A might have been accounted for by the increased insulin sensitivity and suppression of genes that are involved in hepatic gluconeogenesis and lipogenesis. In summary, we have uncovered a new class of non-steroidal FXR agonist that shows promise in treating NAFLD and the associated metabolic syndrome.

Introduction

Farnesoid X receptor (FXR, or NR1H4), a member of the nuclear receptor subfamily, is highly expressed in the liver, intestine, kidney and adrenal gland (Forman et al., 1995). Once activated, FXR binds to the FXR response elements (FXREs) to regulate target gene transcription. Bile acids are the endogenous FXR ligands (Makishima et al., 1999; Parks et al., 1999; Wang et al., 1999). When activated by bile acids, FXR stimulates the expression of small heterodimer partner (SHP) in the liver and executes a negative feedback regulation on the synthesis of bile acids by inhibiting the rate-limiting enzyme cholesterol-7α-hydroxylase (CYP7A1) and increasing the expression of bile salt export protein (BSEP) to maintain the homeostasis of bile acids and cholesterol (Goodwin et al., 2000; Lu et al., 2000).

FXR has been reported to have multiple roles in the pathogenesis of metabolic disorders. Previous studies showed that the FXR knockout (FXR KO) mice exhibited elevated plasma levels of cholesterol and triglycerides and excessive accumulation of fat in the liver (Lambert et al., 2003; Schmitt et al., 2015; Sinal et al., 2000). FXR deficiency also led to impaired glucose tolerance and insulin sensitivity (Ma et al., 2006). Furthermore, hepatic overexpression of constitutively active FXR lowered blood glucose levels in diabetic *db/db* and WT mice (Zhang et al., 2006). In pharmacological models, treatment with the FXR agonists GW4064 (Liu et al., 2003; Zhang et al., 2006) or 6-ECDCA (6α-ethyl-chenodeoxycholic acid, a CDCA derivative) (Cipriani et al., 2010; Maneschi et al., 2013) lowered the plasma levels of

4

triglycerides and cholesterol in chow-fed mice, and ameliorated obesity, hepatic

steatosis, hyperglycemia and hyperlipidemia in *db/db* or high-fat diet (HFD)-induced

diabetic mice, rats and rabbits.

Nonalcoholic fatty liver disease (NAFLD) is currently the most prevalent chronic

liver disease worldwide (Loomba and Sanyal, 2013). It is estimated that 30% of

patients with NAFLD may progress to nonalcoholic steatohepatitis (NASH), the

severe form of NAFLD that could further progress to cirrhosis and hepatocellular

carcinoma. However, there are no pharmacological therapies approved for NAFLD.

The primary therapeutic intervention for patients with NAFLD is weight loss through

dietary modification and life style changes (Loomba and Sanyal, 2013). Clearly, there

is an unmet need for the therapies of NAFLD.

Since the majority of pre-clinical data suggested benefits of FXR agonism in

improving glucose homeostasis and lipid metabolism in the liver, FXR agonists have

been explored as potential therapies for NAFLD (Li et al., 2013). Indeed, extensive

efforts have been dedicated to the discovery of FXR agonists for more than a decade

(Ali et al., 2015). Several classes of FXR agonists, including GW4046 (Liu et al.,

2003; Maloney et al., 2000; Zhang et al., 2006), 6-ECDCA (Cipriani et al., 2010;

Maneschi et al., 2013; Mudaliar et al., 2013), WAY-362450 (Flatt et al., 2009; Zhang

et al., 2009) and Px-102 (a GW4046 derivative) (Gege et al., 2014), have been

developed and evaluated for their activities in relieving NAFLD and type 2 diabetes.

6-ECDCA (also known as Obeticholic acid) and Px-102 have entered phase II clinical

trials in patients of NAFLD and type 2 diabetes. However, the clinical data showed

that a chronic use of steroidal Obeticholic acid may produce cholesterol-related side

effects (Armstrong and Newsome, 2015; Trivedi et al., 2016). Therefore, FXR ligands

with non-steroidal chemical structures are urgently needed for the verification of

proposed hypothesis and therapeutic development.

In this study, Altenusin (2076A), a non-steroidal fungal metabolite (Nakanishi et al.,

1995), was discovered as a new class of chemical structure that selectively activates

FXR. 2076A improves lipid and glucose metabolism both *in vitro* and *in vivo*.

Moreover, treatment of mice with 2076A markedly reversed the pre-existing NAFLD

induced by HFD.

Materials and Methods

Animals, diet and drug treatment

Wild-type (WT) and whole body FXR KO male mice in the C57BL/6J background
were purchased from the Jackson Laboratory (Bar Harbor, ME). All mice were
housed under a standard 12-hour light, 12-hour dark cycle with free access to food
and water. The use of mice in this study complied with all relevant federal guidelines
and institutional policies. For the high-fed diet (HFD) model, 6-week-old male mice
were fed with HFD (Cat #S3282) containing 60% of total calories from animal fat
purchased from Bio-Serv (Frenchtown, NJ) for 16 weeks. When necessary, mice were
treated with 2076A isolated by North China Pharmaceutical Group Corporation
(NCPC) in 20% dimethyl sulfoxide (DMSO) by daily intraperitoneal injections, and
the control mice received the vehicle injections. Body composition was analyzed in
live mice using EchoMRI-100TM from Echo Medical Systems (Houston, TX).

Transient transfection and luciferase reporter gene assay

HEK293T cells were used for transient transfection and luciferase reporter gene assay.
For the initial screening, cells co-transfected with pG5-SV40-Luc reporter plasmid,
together with the GAL4 chimeric receptor expression plasmids pGAL4-PPARα-LBD,
pGAL4-PPARδ-LBD, pGAL4-PPARγ-LBD, pGAL4-LXRα-LBD,
pGAL4-FXR-LBD, pGAL4-RXR-LBD, pGAL4-ERα-LBD, pGAL4-GR-LBD,
pGAL4-RARα-LBD, pGAL4-RARβ-LBD, pGAL4-RARγ-LBD, pGAL4-RORα-LBD,
pGAL4-RORβ-LBD, or pGAL4-RORγ-LBD using Lipofectamine 2000 transfection

reagent from Invitrogen (Zheng et al., 2010). Ligands were added to the medium 6 h

after the transfection. The firefly luciferase and Renilla luciferase activities were

measured after another 24 h of incubation using Dual-Luciferase® Reporter Assay

System (Cat #E1910) from Promega (Madison, WI). Luciferase activities were

normalized to renilla activity. For the subsequent confirmation of FXR activation and

testing of CAR activation, cells were co-transfected with plasmids encoding the

full-length human FXR or mouse CAR, and the FXR responsive luciferase reporter

gene tk-EcRE-Luc, or the CAR responsive reporter gene tk-PBRE-Luc. Cells were

harvested 24 h after the drug treatment and measured for luciferase activity.

Transfection efficiency was normalized against β-gal activity derived from the

co-transfected pCMX-β-gal plasmid. Fold inductions were calculated as relative

reporter activity compared to the vehicle treated cells (Gao et al., 2015). The half

maximal effective concentration (EC50) was measured by dose-response fit sigmoidal

nonlinear regression curve of Origin software 7.0 version.

Isolation and culture of primary mouse hepatocytes

Primary mouse hepatocytes were isolated from 6 to 8-week old male mice as

previously described (Gao et al., 2015). Briefly, the liver was first perfused with

Hanks' buffered salt solution containing 0.5 mM EGTA and 0.1 M HEPES at 5

mL/min for 5-10 min and then perfused with L-15 medium containing 1.8 mM $CaCl_2$,

0.1 M HEPES and 20 μg/mL liberase TM (Roche). After perfusion, the dissociated

hepatocytes were filtered through 50-μm pore mesh and collected by centrifugation at

500 rpm for 3 min at 4°C. Hepatocytes were seeded onto type 1 collagen-coated

dishes in William E medium containing 5% fetal bovine serum. The medium was

changed to HepatoZYME-SFM medium (GIBCO) 2 h later.

Hepatocyte glucose production assay

Forskolin-stimulated glucose production in the primary mouse hepatocytes was

measured as described (He et al., 2013). Briefly, hepatocytes were plated onto

collagen-coated six-well plates at the density of 2×10^5 cells per well. After cells

attached for 2 h, the medium was changed to hepatocyte maintenance medium for

overnight. The cells were then washed three times with PBS before incubation for 4 h

in the glucose production medium in the presence or absence of 10 μM forskolin, and

with or without the test compounds. The medium was collected and glucose was

measured using a hexokinase-based glucose assay kit from Sigma. Glucose levels

were normalized to the protein concentrations of the cell lysates.

Real-time PCR analysis

Total RNA was isolated using the TRIzol reagent from Invitrogen. Reverse

transcription was performed with random hexamer primers and Superscript RT III

enzyme from Invitrogen. SYBR Green-based real-time PCR was performed with the

ABI 7300 Real-Time PCR System. The PCR primer sequences are shown in Table 1.

The quantity of mRNA was normalized to the cyclophilin gene.

Glucose and insulin tolerance tests, and glucose-stimulated insulin secretion

(GSIS) analysis

For the intraperitoneal glucose tolerance test (GTT), mice were fasted for 16 h before

receiving an intraperitoneal injection of 2 g/kg glucose, and blood glucose levels were

measured using the Accu-Chek II glucometer from Roche Diagnostics (Indianapolis,

IN) *via* tail vein at the time points of 0, 15, 30, 60, 90, and 120 min. At the same time

points, blood samples were also collected from tail vein and centrifuged, then stored

at -80 °C for the insulin measurements and GSIS analysis. For the insulin tolerance

test (ITT), mice were fasted for 6 h before receiving an intraperitoneal injection of

insulin at 0.5 units/kg body weight, and blood glucose levels were measured at the

time points of 0, 15, 30, 60, 90, and 120 min.

Tissue histology and plasma biochemistry

For H&E staining, tissues were fixed in 10% paraformaldehyde, embedded in paraffin,

sectioned at 5 μm, and stained with hematoxylin and eosin. For plasma biochemistry,

blood samples were collected from mice with heparinized syringes and then

centrifuged at 5000 rpm for 8 min. Plasma samples were stored at -80 °C until further

analysis. Plasma levels of triglycerides, total cholesterol, aspartate aminotransferase

(AST), and alanine aminotransferase (ALT) were measured by using assay kits from

Stanbio Laboratory (Boerne, TX). Plasma insulin levels were measured by using an

assay kit from Crystal Chem (Downers Grove, IL).

Measurement of liver triglyceride and cholesterol contents

Lipids in the liver were extracted and measured as described (He et al., 2013). Briefly,

approximately 100 mg of liver were homogenized with 3 ml of T-PER (Pierce). The

homogenates were used for protein concentration analysis by the Bradford assay from

Bio-Rad (Milan, Italy). To measure the triglyceride and cholesterol contents, 100 μL

of tissue extracts were added to 1.6 mL $CHCl_3$: MeOH (2:1) for 16 h at 4° C. At the

end of incubation, 200 μL of 0.6% NaCl was added and the solutions were

centrifuged at 2,000 g for 20 min. The organic layer was removed and dried, and the

resulting pellet was dissolved in 100 μL phosphate buffered saline containing 0.5%

Triton X-100. Triglyceride and cholesterol concentrations were then measured by

using assay kits from Stanbio Laboratory.

Western blotting

For Western blot analysis, tissues and cells were lysed in ice-cold NP-40 lysis buffer

containing a protease inhibitor cocktail from Roche, and then quantified for protein

concentrations by a bicinchoninic acid (BCA) assay kit from Pierce (Rockford, IL).

Protein samples were resolved by electrophoresis on 10% SDS-polyacrylamide gels.

After transfer of proteins to nitrocellulose membranes, the membranes were probed

with primary antibodies against total AKT (Cat #9272) and phospho-Akt (serine 473)

(Cat #9271) from Cell Signaling. Detection was achieved by using the ECL system

from Amersham (Piscataway, NJ). The signals were quantified by using the Image J

software version 1.47.

Molecular docking

Docking of 2076A into the LBD of FXR was performed using Autodock version 4.2 software from the Scripps Research Institute (La Jolla, CA) (Morris et al., 2009). The crystal structure of human FXR LBD (Protein Data Bank accession code 1OSH) (Downes et al., 2003) was used as the binding protein. 3D structure of 2076A was built and the lowest energy conformer was optimized using ChemDraw Ultra 11 from Cambridge Soft Corporation (Cambridge, MA). The Lamarckian genetic algorithm was employed for docking simulation. The coordinates of the crystalized ligand fexaramine were chosen as active-site center, and a grid box size of 25 Å×25 Å×25 Å was used. The protein was treated as rigid, whereas 2076A was treated as a flexible molecule. Based on the cluster result and the binding energy, the most favorable dock conformation was chosen for further analysis. Illustration of the 3D model was created by using the Pymol software from DeLano Scientific (San Carlos, USA).

Statistical analysis

Data are expressed as mean ± SD. Statistical significance between two groups was determined by unpaired two-tailed Student's t-test. For comparison among multiple groups, one-way ANOVA followed by Dunnett's multiple comparisons test was used. P value < 0.05 is considered to be statistically significant. Graphs were generated with Graphpad Prism version 5.01.

Results

2076A is a selective FXR agonist

In screening for novel FXR agonists, the GAL4-FXR-LBD chimeric receptor was used to assess the activity of test compounds. Altenusin (2076A) (Fig. 1A), a natural product from North China Pharmaceutical Group Corporation (NCPC)'s microbial metabolite library, was found to induce the GAL4-responsive luciferase reporter gene activity in a concentration-dependent manner, with an estimated EC_{50} value of 3.4 ± 0.2 μM (Fig. 1B). The potency and efficacy of 2076A in activating FXR in the same system were similar to those of CDCA ($EC_{50} = 3.8 \pm 0.3$ μM), an endogenous bile acid FXR agonist. When tested across a panel of GAL4 fusion of nuclear receptors, 2076A showed little activity on 14 other receptors at 30 μM, suggesting that 2076A selectively activates FXR (Fig. 1C). The agonistic activity of 2076A on FXR was verified by an independent luciferase reporter system using the full-length FXR and the FXR-responsive tk-EcRE-Luc reporter gene (Fig. 1D). 2076A also had little effect on CAR, which was verified by a reporter system using the full-length mouse CAR and the CAR-responsive tk-PBRE-Luc reporter gene (Fig. 1E).

To further confirm the activation of FXR by 2076A, primary hepatocytes isolated from the WT and FXR KO mice were treated with vehicle, 2076A or CDCA before being measured for the expression of known FXR responsive genes. As shown in Fig. 1F, compared with the vehicle, 2076A dose-dependently induced the expression of small heterodimer partner (SHP), bile salt export pump (BSEP) and scavenger

13

receptor class B1 (SR-B1), three known FXR target genes, and suppressed the

expression of cholesterol-7α-hydroxylase (CYP7A1), a gene negatively regulated by

FXR (Goodwin et al., 2000; Lu et al., 2000), in hepatocytes isolated from WT mice,

whereas these responses were abolished in hepatocytes isolated from FXR KO mice.

Computational docking analysis of the binding of 2076A to FXR

To determine whether 2076A can bind to FXR, we performed a molecular docking

simulation by using the Autodock 4.2 software and the crystal structure of the human

FXR LBD (Downes et al., 2003). In the dominant conformational cluster, the

conformation with the lowest binding energy was used to predict the binding mode.

As shown in Fig. 2, 2076A fits well into the ligand-binding pocket of FXR. The

hydroxyl-, methoxy-, and carboxyl- groups of 2076A were able to establish several

hydrogen bond contacts with four amino acids in the ligand-binding pocket, His298,

Ser336, Leu352 and Tyr365. In addition to hydrogen bonds, multiple hydrophobic

interactions were also observed between 2076A and several amino acids within the

pocket, namely Met294, Met332, Phe340, Ile356 and Met369. These results

suggested that 2076A can bind to the LBD of FXR to activate FXR.

Treatment with 2076A leads to metabolic benefits in chow-fed mice

We went on to investigate whether 2076A could produce metabolic benefits *in vivo*.

We first treated chow-fed WT mice daily with increasing doses of 2076A (5, 10, 30

mg/kg) by intraperitoneal injections for one week. As shown in Fig. 3 and at the dose

14

of 30 mg/kg, treatment with 2076A lowered the levels of fed and fasting blood glucose and plasma triglycerides. Based on these results, we chose the dose of 30 mg/kg for the subsequent *in vivo* experiments. All three doses of 2076A had little effect on the body weight, the ratio of liver to body weight, or the plasma levels of ALT and AST (data not shown), suggesting that 2076A was well tolerated by mice without noticeable toxicity.

Treatment with 2076A inhibits HFD-induced obesity

To further investigate the metabolic benefit of 2076A and its dependence on FXR, we challenged WT and FXR KO male mice with HFD for 16 weeks beginning at the age of 6 weeks, and then treated the mice with 2076A (30 mg/kg) daily by intraperitoneal injections for three weeks during which the mice were remained on HFD. The results showed that the average weight of WT mice treated with 2076A decreased by 22.9 % compared with their vehicle-treated counterparts without significant difference in food intake (data not shown), but this effect was abolished in FXR KO mice (Fig. 4A and 4C). Necropsy showed that the visceral fat mass and subcutaneous fat mass were remarkably lowered in 2076A-treated WT mice but not in 2076A-treated FXR KO mice (Fig. 4B). Body composition analysis by MRI further revealed that treatment with 2076A reduced the fat mass of WT mice from an average of 17.1 ± 2.8 g to 8.5 ± 4.8 g (a reduction of approximately 50%), but had little effect on the lean mass in WT mice (Fig. 4C). These results suggested that the majority of the reduced body weight in 2076A-treated WT mice was accounted for by the decrease of fat mass.

15

Histopathological analysis of the visceral fat by H&E staining showed that the sizes

of adipocytes in 2076A-treated WT mice, but not in 2076A-treated FXR KO mice,

were reduced (Fig. 4D).

To understand the mechanism for the metabolic benefit, we analyzed the expression

of genes involved in energy expenditure and lipogenesis. Uncoupling proteins (UCPs)

are a subgroup of mitochondrial carrier proteins that can affect energy expenditure.

UCP2 and UCP3 are two key regulators of mitochondrial energy metabolism (Boss et

al., 2000). The expression of UCP2 and UCP3 was significantly increased in the

adipose tissue and skeletal muscle of 2076A-treated WT mice but not the FXR KO

mice (Fig. 4E). When the adipose expression of genes involved in adipocyte

differentiation and lipogenesis was analyzed, we found the mRNA levels of

peroxisome proliferator-activated receptor γ (PPARγ) and adipocyte protein 2 (aP2),

two key adipocyte differentiation markers (MacDougald and Lane, 1995), were

significantly decreased in 2076A-treated WT mice but not the FXR KO mice (Fig.

4F). The expression of lipogenic genes acetyl-CoA carboxylase (ACC), fatty acid

synthase (FAS) and sterol-regulatory-element binding protein-1c (SREBP-1c) was

down-regulated in 2076A-treated WT mice but not the FXR KO mice (Fig. 4G).

Treatment with 2076A reverses HFD-induced hepatic steatosis

Next, we examined the effect of 2076A on HFD-induced hepatic steatosis. Upon the

19-week HFD feeding and as expected, the vehicle-treated WT mice displayed

16

marked hepatic steatosis, which was supported by both the gross appearance of the

liver (Fig. 5A) and histological analysis by H&E staining (Fig. 5B). Administration

with 2076A for three weeks, while the mice were remained on HFD, almost

completely reversed the lipid droplet accumulation and macrovesicular steatosis in

WT, but not in FXR KO mice (Fig. 5B). Compared with the vehicle control, treatment

with 2076A decreased the liver weight from 1.5 ± 0.3 g to 1.1 ± 0.1 g in WT mice, but

not in FXR KO mice (Fig. 5C). When the lipid contents were analyzed, we found both

the hepatic triglyceride (Fig. 5D) and cholesterol (Fig. 5E) contents in 2076A-treated

WT mice were reduced to approximately half of the vehicle group levels, and these

effects were not seen in 2076A-treated FXR KO mice. These data demonstrated that

2076A could reverse pre-existing hepatic steatosis in a FXR-dependent manner.

Treatment of primary mouse hepatocytes with 2076A also inhibited oleic

acid-induced steatosis *in vitro* (data not shown).

In understanding the mechanism by which 2076A inhibits hepatic steatosis, we found

the expression of lipogenic genes MACD, ACC, FAS, SREBP-1c and liver fatty

acid-binding protein (L-FABP) was all significantly suppressed in the livers of

2076A-treated WT mice, but not in the FXR KO mice (Fig. 5F). L-FABP, highly

expressed in the hepatocytes, can function as a metabolic sensor by regulating the

expression of SREBP-1c, PPARγ and C/EBPα (Chen et al., 2013). These results

suggested that 2076A inhibits hepatic lipogenesis by suppressing the lipogenic gene

expression.

17

Treatment with 2076A alleviates HFD-induced hyperglycemia, hyperinsulinemia and insulin resistance

The chronic HFD model is associated with hallmarks of metabolic syndrome, such as hyperglycemia, hyperinsulinemia and insulin resistance. Indeed, the 19-week HFD feeding in WT mice resulted in hyperglycemia with a fasting blood glucose level of 178.3 ± 12.4 mg/dL (Fig. 6A) and hyperinsulinemia with a serum insulin level of 1.4 ± 0.6 ng/dL (Fig. 6B). Upon 3-week treatment of 2076A, the plasma levels of glucose and insulin in WT mice were decreased to 116.2 ± 4.1 mg/dL (Fig. 6A) and 0.4 ± 0.1 ng/dL (Fig. 6B), respectively, and these effects were not seen in the FXR KO mice, suggesting that 2076A may have lowered the plasma glucose level by increasing the insulin sensitivity. Treatment with 2076A also lowered the serum level of cholesterol (Fig. 6C), but had little effect on the serum level of triglycerides (Fig. 6D) in WT mice.

To determine the effect of 2076A on glucose tolerance and insulin sensitivity, we also performed glucose tolerance (GTT), insulin tolerance (ITT), and glucose stimulated insulin secretion (GSIS) tests. Compared with the vehicle-treated groups, treatment of HFD-fed WT mice, but not the HFD-fed FXR KO mice, with 2076A significantly enhanced the ability of mice to clear the exogenous glucose in GTT (Fig. 6E) and improved their response to insulin to dispose glucose in ITT (Fig. 6F). The GSIS results showed that the 2076A-treated WT mice showed attenuated glucose stimulated

18

insulin secretion (Fig. 6G), consistent with their better performances in GTT and ITT.

Treatment with 2076A had little effect on the morphology and volume of the

pancreatic islets (data not shown). These results suggested that 2076A alleviates

hyperglycemia and hyperinsulinemia, and improves insulin sensitivity in diabetic

mice in a FXR-dependent manner.

Treatment with 2076A sensitizes insulin signaling and inhibits hepatic

gluconeogenesis *in vitro* and *in vivo*

To understand the molecular mechanism underlying the anti-diabetic effect of 2076A,

we investigated the effect of 2076A on insulin signaling by measuring the

phosphorylation of AKT at Ser473, a phosphorylation site required for downstream

propagation of the insulin signaling (Hernandez et al., 2001). *In vitro*, treatment of

primary mouse hepatocytes with 2076A in the absence (Fig. 7A) or presence (Fig. 7B)

of insulin (100 nM) robustly increased the AKT phosphorylation. *In vivo*, treatment of

WT mice with 2076A increased the phosphorylation of AKT in the liver and skeletal

muscle, but not in the white adipose tissue (WAT) (Fig. 7C).

Increased hepatic gluconeogenesis is an important pathogenic event in the

development of diabetes (Barthel and Schmoll, 2003), so we next investigated the

effect of 2076A on hepatic gluconeogenesis. Treatment of primary mouse hepatocytes

with 2076A dose-dependently inhibited forskolin-induced glucose production (Fig.

7D). *In vivo*, treatment with 2076A significantly suppressed the expression of hepatic

19

gluconeogenic genes, including forkhead box protein O1 (FoxO1),

phosphoenolpyruvate carboxykinase (PEPCK), glucose-6-phosphatase (G6Pase) and

peroxisome proliferator-activated receptor-γ coactivator-1α (PGC-1α) in WT but not

in FXR KO mice (Fig. 7E).

20

Discussion

In this report, we have discovered a new class of non-steroidal FXR agonist 2076A that exhibits marked metabolic benefits. Administration of 2076A to HFD-induced obese mice resulted in significant reductions in body weight and fat mass, alleviation of dyslipidemia and insulin resistance, and reversal of hepatic steatosis. The metabolic benefits of 2076A were abolished in FXR KO mice, suggesting that FXR is the mediator of these effects.

2076A is a fungal metabolite that was originally purified as a weak inhibitor of the myosin light-chain kinase from the endophytic fungal strain *Alternaria sp*. This fungal strain was isolated from the leaves of medicinal plant *polygonumse negalense* in Egypt (Nakanishi et al., 1995). 2076A was subsequently reported to have other bioactivities, such as radical scavenging and antifungal (Johann et al., 2012; Wang et al., 2012). The present study has provided compelling evidence that 2076A is a novel class of FXR agonist.

FXR plays critical roles in maintaining the homeostasis of bile acids, lipid and glucose by regulating the transcription of genes involved in lipid and glucose homeostasis and inflammation. However, the metabolic benefits of FXR are not without controversies. For example, it has been reported that the HFD-fed FXR whole-body KO mice displayed metabolic improvement (Gonzalez et al., 2015; Prawitt et al., 2011), and glycine-β-muricholic acid, a bile acid derivative and FXR antagonist, exhibited metabolic benefits in diet-induced and genetic obese mice

21

through intestine-selective FXR antagonism (Jiang et al., 2015). However, the

majority of previous studies demonstrated the metabolic benefits of FXR agonists,

such as PX-102 and Obeticholic acid, in improving glucose homeostasis and lipid

metabolism. PX-102, a derivative of GW4064 with improved ADME properties

(Gege et al., 2014), is currently tested in a phase IIa study in patients with NAFLD

(https://www.clinicaltrials.gov). Obeticholic acid (also known as 6-ECDCA and

INT-767), a semisynthetic FXR agonist derived from CDCA, has been shown to have

therapeutic benefits, including improving lipid and glucose homeostasis,

anti-inflammation and anti-fibrosis in the liver, kidney and intestine (Cipriani et al.,

2010; Mudaliar et al., 2013). Obeticholic acid was recently approved by FDA for the

treatment of primary biliary cirrhosis and became the first-in class FXR agonist drug

(Trivedi et al., 2016). In addition, Obeticholic acid showed promising results in a

phase IIb clinical trial in patients with type 2 diabetes, NAFLD and NASH

(Armstrong and Newsome, 2015; Mudaliar et al., 2013). Consistent with these notions,

the current study demonstrated that activation of FXR by 2076A can relieve metabolic

disorder in mice.

The FXR-dependent anti-obesity and anti-steatotic activity of 2076A was consistent

with previous reports that FXR agonists lowered plasma levels of cholesterol and

triglyceride and decreased accumulation of fat in the liver (Cipriani et al., 2010; Liu et

al., 2003; Maneschi et al., 2013; Zhang et al., 2006). The suppression of lipogenic

genes in 2076A-treated WT mice was consistent with the observation that the

expression of lipogenic genes was up-regulated in FXR KO mice (Ma et al., 2006).

The alleviation of hyperglycemia and hyperinsulinemia and improved insulin

sensitivity in HFD-induced obese and diabetic mice by 2076A was consistent with the

report that FXR deficiency led to impaired glucose tolerance and insulin sensitivity in

mice and rats (Ma et al., 2006). The inhibition of gluconeogenesis by 2076A was also

consistent with a previous report that FXR KO mice had elevated expression of

gluconeogenic genes (Ma et al., 2006).

2076A is a selective FXR agonist but has little activity on 15 other nuclear receptors,

among which is the xenobiotic receptor CAR. We and others reported that activation

of CAR inhibits obesity and relieves insulin resistance (Dong et al., 2009; Gao et al.,

2009). The lack of CAR activation suggested that CAR does not contribute to the

metabolic benefit of 2076A. The G protein-coupled bile acid receptor (TGR5) is a

member of the G-protein-coupled receptor (GPCR) superfamily. Activation of TGR5

by bile acids or synthetic ligands has been shown to be beneficial in body weight

maintenance and glucose metabolism (Chen et al., 2011; Wang et al., 2011). Our

results showed that 2076A had little effect on the hepatic expression of TGR5 *in vivo*.

Moreover, treatment of TGR5-transfected cells with 2076A failed to activate the

co-transfected TGR5 responsive reporter gene pCRE-luc (data not shown). 2076A is a

non-bile acid compound, and its metabolic benefits were abolished in FXR KO mice.

These results suggest that the metabolic benefits of 2076A is FXR-dependent but

TGR5-independent. FXR has also been reported to induce the expression of FGF21 in

23

rats and HepG2 cells (Cyphert et al., 2012). It will be interesting to know whether the

induction of FGF21 by FXR is conserved in mice and if so, whether the induction of

FGF21 contributes to the anti-obesity effect of 2076A. There is also growing evidence

that microbiome is an important contributor to NAFLD (Quigley et al., 2016), and

FXR has been shown to impact gut microbiota (Gonzalez et al., 2016; Zhang et al.

2016). Future studies are necessary to determine whether 2076A can alter the

composition of microbiome.

In summary, we have discovered the natural product 2076A as a new class of

non-steroidal FXR agonist with marked metabolic benefits. The distinct

pharmacophore of 2076A provides much needed opportunities to target FXR for the

treatment of NAFLD and associated metabolic syndrome.

Conflicts of Interest

The authors declare no conflicts of interest.

Author Contributions

Participated in research design: Z. Zheng, Z. Zhao, W. Xie.

Conducted experiments: Z. Zheng, Z. Zhao, X. Lu, W. Shen, M. Jiang, J. Lin, Y. An, Y. Xie, M. Xu, Y. Huang.

Performed data analysis: Z. Zheng, Z. Zhao, W. Xie.

Wrote or contributed to writing of the manuscript: Z. Zheng, Z. Zhao, W. Shen, S. Li, G. L. Guo, S. Li, X. Zhang, W. Xie.

References

Ali AH, Carey EJ and Lindor KD (2015) Recent advances in the development of
farnesoid X receptor agonists. *Ann Transl Med* **3**: 5.

Armstrong MJ and Newsome PN (2015) Trials of obeticholic acid for non-alcoholic
steatohepatitis. *Lancet* **386**: 28.

Barthel A and Schmoll D (2003) Novel concepts in insulin regulation of hepatic
gluconeogenesis. *Am J Physiol Endocrinol Metab* **285**: E685-692.

Boss O, Hagen T and Lowell BB (2000) Uncoupling proteins 2 and 3: potential
regulators of mitochondrial energy metabolism. *Diabetes* **49**: 143-156.

Chen A, Tang Y, Davis V, Hsu FF, Kennedy SM, Song H, Turk J, Brunt EM,
Newberry EP and Davidson NO (2013) Liver fatty acid binding protein
(L-Fabp) modulates murine stellate cell activation and diet-induced
nonalcoholic fatty liver disease. *Hepatology* **57**: 2202-2212.

Chen X, Lou G, Meng Z, and Huang W (2011) TGR5: a novel target for weight
maintenance and glucose metabolism. *Exp Diabetes Res* **2011:** 853501

Cipriani S, Mencarelli A, Palladino G and Fiorucci S (2010) FXR activation reverses
insulin resistance and lipid abnormalities and protects against liver steatosis in
Zucker (fa/fa) obese rats. *J Lipid Res* **51**: 771-784.

Cyphert HA, Ge X, Kohan AB, Salati LM, Zhang Y, Hillgartner FB (2012)
Activation of the farnesoid X receptor induces hepatic expression and secretion
of fibroblast growth factor 21. *J Biol Chem* **287:** 25123-25138.

Dong B, Saha PK, Huang W, Chen W, Abu-Elheiga LA, Wakil SJ, Stevens RD,

Ilkayeva O, Newgard CB, Chan L, and Moore DD (2009) Activation of nuclear receptor CAR ameliorates diabetes and fatty liver disease. *Proc Natl Acad Sci U S A* **106:** 18831-18836.

Downes M, Verdecia MA, Roecker AJ, Hughes R, Hogenesch JB, Kast-Woelbern HR, Bowman ME, Ferrer JL, Anisfeld AM, Edwards PA, Rosenfeld JM, Alvarez JG, Noel JP, Nicolaou KC and Evans RM (2003) A chemical, genetic, and structural analysis of the nuclear bile acid receptor FXR. *Mol Cell* **11**: 1079-1092.

Flatt B, Martin R, Wang TL, Mahaney P, Murphy B, Gu XH, Foster P, Li J, Pircher P, Petrowski M, Schulman I, Westin S, Wrobel J, Yan G, Bischoff E, Daige C and Mohan R (2009) Discovery of XL335 (WAY-362450), a highly potent, selective, and orally active agonist of the farnesoid X receptor (FXR). *J Med Chem* **52**: 904-907.

Forman BM, Goode E, Chen J, Oro AE, Bradley DJ, Perlmann T, Noonan DJ, Burka LT, McMorris T, Lamph WW, Evans RM and Weinberger C (1995) Identification of a nuclear receptor that is activated by farnesol metabolites. *Cell* **81**: 687-693.

Gao J, He J, Zhai Y, Wada T, and Xie W (2009) The constitutive androstane receptor is an anti-obesity nuclear receptor that improves insulin sensitivity. *J Biol Chem* **284**: 25984-25992.

Gao J, Yan J, Xu M, Ren S and Xie W (2015) CAR Suppresses Hepatic Gluconeogenesis by Facilitating the Ubiquitination and Degradation of

PGC1alpha. *Mol Endocrinol* **29**: 1558-1570.

Gege C, Kinzel O, Steeneck C, Schulz A and Kremoser C (2014) Knocking on FXR's door: the "hammerhead"-structure series of FXR agonists - amphiphilic isoxazoles with potent in vitro and in vivo activities. *Curr Top Med Chem* **14**: 2143-2158.

Gonzalez FJ, Jiang C, Bisson WH and Patterson AD (2015) Inhibition of farnesoid X receptor signaling shows beneficial effects in human obesity. *J Hepatol* **62**: 1234-1236.

Gonzalez FJ, Jiang C, Patterson AD (2016) An intestinal microbiota-farnesoid X receptor axis modulates metabolic disease. *Gastroenterology*. **151:** 845-859.

Goodwin B, Jones SA, Price RR, Watson MA, McKee DD, Moore LB, Galardi C, Wilson JG, Lewis MC, Roth ME, Maloney PR, Willson TM and Kliewer SA (2000) A regulatory cascade of the nuclear receptors FXR, SHP-1, and LRH-1 represses bile acid biosynthesis. *Mol Cell* **6**: 517-526.

He J, Gao J, Xu M, Ren S, Stefanovic-Racic M, O'Doherty RM and Xie W (2013) PXR ablation alleviates diet-induced and genetic obesity and insulin resistance in mice. *Diabetes* **62**: 1876-1887.

Hernandez R, Teruel T and Lorenzo M (2001) Akt mediates insulin induction of glucose uptake and up-regulation of GLUT4 gene expression in brown adipocytes. *FEBS Lett* **494**: 225-231.

Jiang C, Xie C, Lv Y, Li J, Krausz KW, Shi J, Brocker CN, Desai D, Amin SG, Bisson WH, Liu Y, Gavrilova O, Patterson AD and Gonzalez FJ (2015)

Intestine-selective farnesoid X receptor inhibition improves obesity-related metabolic dysfunction. *Nat Commun* **6**: 10166.

Johann S, Rosa LH, Rosa CA, Perez P, Cisalpino PS, Zani CL and Cota BB (2012) Antifungal activity of altenusin isolated from the endophytic fungus Alternaria sp. against the pathogenic fungus Paracoccidioides brasiliensis. *Rev Iberoam Micol* **29**: 205-209.

Lambert G, Amar MJ, Guo G, Brewer HB, Jr., Gonzalez FJ and Sinal CJ (2003) The farnesoid X-receptor is an essential regulator of cholesterol homeostasis. *J Biol Chem* **278**: 2563-2570.

Li Y, Jadhav K, and Zhang Y (2013) Bile acid receptors in non-alcoholic fatty liver disease. *Biochem Pharmacol* **86:** 1517-1524

Liu Y, Binz J, Numerick MJ, Dennis S, Luo G, Desai B, MacKenzie KI, Mansfield TA, Kliewer SA, Goodwin B and Jones SA (2003) Hepatoprotection by the farnesoid X receptor agonist GW4064 in rat models of intra- and extrahepatic cholestasis. *J Clin Invest* **112**: 1678-1687.

Loomba R and Sanyal AJ (2013) The global NAFLD epidemic. *Nat Rev Gastroenterol Hepatol* **10**: 686-690.

Lu TT, Makishima M, Repa JJ, Schoonjans K, Kerr TA, Auwerx J and Mangelsdorf DJ (2000) Molecular basis for feedback regulation of bile acid synthesis by nuclear receptors. *Mol Cell* **6**: 507-515.

Ma K, Saha PK, Chan L and Moore DD (2006) Farnesoid X receptor is essential for normal glucose homeostasis. *J Clin Invest* **116**: 1102-1109.

MacDougald OA and Lane MD (1995) Transcriptional regulation of gene expression

during adipocyte differentiation. *Annu Rev Biochem* **64**: 345-373.

Makishima M, Okamoto AY, Repa JJ, Tu H, Learned RM, Luk A, Hull MV, Lustig

KD, Mangelsdorf DJ and Shan B (1999) Identification of a nuclear receptor

for bile acids. *Science* **284**: 1362-1365.

Maloney PR, Parks DJ, Haffner CD, Fivush AM, Chandra G, Plunket KD, Creech KL,

Moore LB, Wilson JG, Lewis MC, Jones SA and Willson TM (2000)

Identification of a chemical tool for the orphan nuclear receptor FXR. *J Med

Chem* **43**: 2971-2974.

Maneschi E, Vignozzi L, Morelli A, Mello T, Filippi S, Cellai I, Comeglio P,

Sarchielli E, Calcagno A, Mazzanti B, Vettor R, Vannelli GB, Adorini L and

Maggi M (2013) FXR activation normalizes insulin sensitivity in visceral

preadipocytes of a rabbit model of MetS. *J Endocrinol* **218**: 215-231.

Morris GM, Huey R, Lindstrom W, Sanner MF, Belew RK, Goodsell DS and Olson

AJ (2009) AutoDock4 and AutoDockTools4: Automated docking with

selective receptor flexibility. *J Comput Chem* **30**: 2785-2791.

Mudaliar S, Henry RR, Sanyal AJ, Morrow L, Marschall HU, Kipnes M, Adorini L,

Sciacca CI, Clopton P, Castelloe E, Dillon P, Pruzanski M and Shapiro D

(2013) Efficacy and safety of the farnesoid X receptor agonist obeticholic acid

in patients with type 2 diabetes and nonalcoholic fatty liver disease.

Gastroenterology **145**: 574-582 e571.

Nakanishi S, Toki S, Saitoh Y, Tsukuda E, Kawahara K, Ando K and Matsuda Y

30

(1995) Isolation of myosin light chain kinase inhibitors from microorganisms: dehydroaltenusin, altenusin, atrovenetinone, and cyclooctasulfur. *Biosci Biotechnol Biochem* **59**: 1333-1335.

Parks DJ, Blanchard SG, Bledsoe RK, Chandra G, Consler TG, Kliewer SA, Stimmel JB, Willson TM, Zavacki AM, Moore DD and Lehmann JM (1999) Bile acids: natural ligands for an orphan nuclear receptor. *Science* **284**: 1365-1368.

Prawitt J, Abdelkarim M, Stroeve JH, Popescu I, Duez H, Velagapudi VR, Dumont J, Bouchaert E, van Dijk TH, Lucas A, Dorchies E, Daoudi M, Lestavel S, Gonzalez FJ, Oresic M, Cariou B, Kuipers F, Caron S and Staels B (2011) Farnesoid X receptor deficiency improves glucose homeostasis in mouse models of obesity. *Diabetes* **60**: 1861-1871.

Quigley EM, Abu-Shanab A, Murphy EF, Stanton C, Monsour HP Jr (2016) The metabolic role of the microbiome: implications for NAFLD and the metabolic syndrome. *Semin Liver Dis* **36:** 312-316.

Schmitt J, Kong B, Stieger B, Tschopp O, Schultze SM, Rau M, Weber A, Mullhaupt B, Guo GL and Geier A (2015) Protective effects of farnesoid X receptor (FXR) on hepatic lipid accumulation are mediated by hepatic FXR and independent of intestinal FGF15 signal. *Liver Int* **35**: 1133-1144.

Sinal CJ, Tohkin M, Miyata M, Ward JM, Lambert G and Gonzalez FJ (2000) Targeted disruption of the nuclear receptor FXR/BAR impairs bile acid and lipid homeostasis. *Cell* **102**: 731-744.

Trivedi PJ, Hirschfield GM and Gershwin ME (2016) Obeticholic acid for the

31

treatment of primary biliary cirrhosis. *Expert Rev Clin Pharmacol* **9**: 13-26.

Wang H, Chen J, Hollister K, Sowers LC and Forman BM (1999) Endogenous bile

acids are ligands for the nuclear receptor FXR/BAR. *Mol Cell* **3**: 543-553.

Wang QX, Bao L, Yang XL, Guo H, Yang RN, Ren B, Zhang LX, Dai HQ, Guo LD

and Liu HW (2012) Polyketides with antimicrobial activity from the solid

culture of an endolichenic fungus Ulocladium sp. *Fitoterapia* **83**: 209-214.

Wang YD, Chen WD, Yu D, Forman BM, and Huang W (2011) The G-protein-coupled

bile acid receptor, Gpbar1 (TGR5), negatively regulates hepatic inflammatory

response through antagonizing nuclear factor κ light-chain enhancer of

activated B cells (NF-κB) in mice. *Hepatology* **54**: 1421-1432.

Zhang L, Xie C, Nichols RG, Chan SH, Jiang C, Hao R, Smith PB, Cai J, Simons MN,

Hatzakis E, Maranas CD, Gonzalez FJ, Patterson AD (2016) Farnesoid X

receptor signaling shapes the gut microbiota and controls hepatic lipid

metabolism. *mSystems* **1. pii:** e00070-16.

Zhang S, Wang J, Liu Q and Harnish DC (2009) Farnesoid X receptor agonist

WAY-362450 attenuates liver inflammation and fibrosis in murine model of

non-alcoholic steatohepatitis. *J Hepatol* **51**: 380-388.

Zhang Y, Lee FY, Barrera G, Lee H, Vales C, Gonzalez FJ, Willson TM and Edwards

PA (2006) Activation of the nuclear receptor FXR improves hyperglycemia

and hyperlipidemia in diabetic mice. *Proc Natl Acad Sci U S A* **103**:

1006-1011.

Zheng ZH, Lu XH, Zhang H, Lv GP, He JG, Zhao BH and Si SY (2010) Impacts of

different promoters on the mammalian one-hybrid assay for detecting nuclear

receptor agonists. *Anal Bioanal Chem* **396**: 1721-1730.

Footnotes

2. Z. Zheng and Z. Zhao contributed equally to this work.

34

Figure Legends

Figure 1: 2076A is a selective FXR agonist.

(A) Chemical structure of 2076A. **(B)** Activation of the GAL4-hFXR LBD chimeric receptor by 2076A. Cells were co-transfected with GAL4-hFXR LBD and the GAL4-responisve luciferase report tk-UAS-Luc. The transfected cells were treated with increasing concentrations of 2076A for 24 h before luciferase assay. **(C)** 2076A did not activate GAL4 fusions of 14 other nuclear receptors. **(D)** Activation of the full-length FXR by 2076A. Cells were co-transfected with FXR and the FXR-responsive tk-EcRE-Luc luciferase report gene. The transfected cells were treated with increasing concentrations of 2076A for 24 h before luciferase assay. **(E)** Lack of activation of CAR by 2076A. Cells were co-transfected with the full-length mouse CAR and the CAR-responsive tk-PBRE-Luc luciferase report. The transfected cells were treated with 2076A or TCPOBOP (TC) for 24 h before luciferase assay. **(F)** The expression of FXR responsive genes in primary hepatocytes isolated from wild-type (WT) and FXR knockout (KO) mice. The hepatocytes were treated with vehicle or 2076A (10, 25 or 50 μM) for 24 h before cell harvesting and real-time PCR analysis, CDCA (50 μM) was included as the positive control. The data represent mean ± SD. n = 3 for each group. *, $P < 0.05$; **, $P < 0.01$ compared with the vehicle treated group. The transfection results represent one of three independent experiments.

Figure 2: Computational docking analysis of the binding of 2076A to FXR.

The docking analysis was based on the crystal structures of human FXR from the

Protein Data Bank (PDB id: 1OSH). The hydrogen bond interactions between 2076A

and FXR are shown in yellow dash lines.

Figure 3: Treatment with 2076A leads to metabolic benefits in chow-fed mice.

Eight-week old WT mice fed on chow-diet were treated daily with increasing doses of

2076A (5, 10, 30 mg/kg) by intraperitoneal injections for one week, the fed blood

glucose and fasting blood glucose levels were measured. The plasma concentrations

of triglyceride and cholesterol were also measured. n = 4 for each group, *, $P < 0.05$,

compared with the vehicle-treated group.

Figure 4: Treatment with 2076A inhibits HFD-induced obesity.

WT (n = 4 for each group) and FXR KO mice (n = 5 for each group) were fed with

HFD for 16 weeks and then treated intraperitoneally with 2076A (30 mg/kg/day) for

three weeks. **(A)** Representative appearance of mice at the end of the experiment. **(B)**

Representative appearance of visceral of mice. **(C)** Body weight and body

composition analysis. **(D)** Histological analysis of the visceral fat by H&E staining.

(E, F and G) The mRNA expression of mitochondrial uncoupling proteins UCPs in

the white adipose tissue and skeletal muscle (E), adipocyte differentiation marker

genes (F) and lipogenic genes (G) in the visceral fat was measured by real-time PCR.

*, $P < 0.05$; **, $P < 0.01$; ***, $P < 0.001$, compared with the vehicle-treated group.

Note only the differences between vehicle group and 2076A treated group within the

36

same genotype (wild-type or FXR knockout) were compared, so the unpaired

two-tailed Student's *t*-test was used.

Figure 5: Treatment with 2076A reverses HFD-induced hepatic steatosis.

Mice were the same as described in Figure 4. **(A)** Appearance of the livers at the end

of the experiment. **(B)** Histological analysis of liver sections by H&E staining. **(C)**

Liver weight **(**left**)** and the ratio of liver weight to body weight **(**right**)**. **(D and E)** The

hepatic levels of triglycerides (D) and cholesterol (E). **(F)** The hepatic mRNA

expression of genes involved in lipogenesis was measured by real-time PCR. WT, n =

4 for each group; FXR KO, n = 5 for each group. *, $P < 0.05$; **, $P < 0.01$, compared

with the vehicle-treated group.

Figure 6: Treatment with 2076A alleviates HFD-induced hyperglycemia,

hyperinsulinemia and insulin resistance.

Mice were the same as described in Figure 4. **(A)** Fasting blood glucose level. **(B)**

Fasting serum insulin level. **(C)** Serum cholesterol level. **(D)** Serum triglyceride level.

(E to G) Glucose tolerance test (GTT, E), insulin tolerance test (ITT, F), and

glucose-stimulated insulin secretion (GSIS) test (G). The GTT, ITT and GSIS results

were also quantified as the area under the curve (AUC). WT, n = 4 for each group;

FXR KO, n = 5 for each group. *, $P < 0.05$; **, $P < 0.01$, compared with the

vehicle-treated group.

Figure 7: Treatment with 2076A sensitizes insulin signaling and inhibits hepatic gluconeogenesis *in vitro* and *in vivo*.

(A) Treatment of primary hepatocytes with 2076A increased the basal phosphorylation of Akt (p-AKT) as shown by Western blotting. Shown on the right is the densitometric quantification of the blots. **(B)** Treatment of primary hepatocytes with 2076A elevated the insulin-stimulated phosphorylation of Akt (p-AKT) as shown by Western blotting. Shown on the right is the densitometric quantification of the blots. **(C)** WT mice were treated with vehicle or 2076A (30 mg/kg/day) for one week before tissue harvesting and measurement of p-AKT in the liver, WAT, and skeletal muscle. Shown on the right is the densitometric quantification of the blots. **(D)** The inhibitory effect of 2076A on the forskolin-stimulated glucose production in primary hepatocytes isolated from WT mice. **(E)** The effect of 2076A on the hepatic expression of gluconeogenic genes in WT (n = 4) and FXR KO (n = 5) mice. *, $P < 0.05$; **, $P < 0.01$, compared with the vehicle-treated group.

Table 1. Primer sequences for real-time PCR

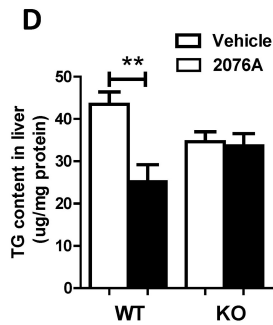| Genes	Forward Primer Sequence (5' - 3')	Reverse Primer Sequence (5' - 3')
ACC	TGACAGACTGATCGCAGA	TGGAGAGCCCCACACAC
aP2	GATGAAATCACCGCAGACG	ATTGTGGTCGACTTTCCAT
BSEP	GGAGATGGCACAGGAGG	GCCCGTAGTGCTTCAGCT
Cyclophilin	AAGGACAGCCACACCAAC	CCAGAACATGACAAACG
CYP7A1	AGCAACTAAACAACCTGCCA	GTCCGGATATTCAAGGATG
FAS	GCTGCGGAAACTTCAGGA	AGAGACGTGTCACTCCTGG
FOXO1	TGGACATGCTCAGCAGACATC	TTGGGTCAGGCGGTTCA
G6Pase	ATGGAGGAAGGAATGAACA	TGGGAAAGAGGACATAGAA
L-FABP	ACCTCATCCAGAAAGGGA	ACAATGTCGCCCAATGTCATG
MACD	ATTTGGAAAGCTGCTAGTGGA	CATAGCCTCCGAAAATCTG
PEPCK	CTCACTGACTCGGCTTACG	CCACTGAATGCAGACACTT
PGC-1α	AAACTTGCTAGCGGTCCTCA	TGGCTGGTGCCAGTAAGAG
PPARγ	GCCCTTTGGTGACTTTATGGA	GCAGCAGGTTGTCTTGGATG
SHP	TGGGTCCCAAGGAGTATGC	CAGTGATGTCAACGTCTCC
SR-B1	CCTTCAATGACAACGACACCG	CCATGCGACTTGTCAGGCT
SREBP1c	ATCGGCGCGGAAGCTGTCGG	ACTGTCTTGGTTGTTGATGA
UCP2	CTCAGAAAGGTGCCTCCCGA	CTCGCTCCTGGAAGATGGTG
UCP3	CCTACGACATCATCAAGGAGA	TCCAAAGGCAGAGACAAAG

39

Figure 1

Figure 2

Figure 3

A

WT   KO

Vehicle   2076A   Vehicle   2076A

B

WT   KO

Vehicle   2076A   Vehicle   2076A

C

D

WT   KO

Vehicle

2076A

E

F

G

A

WT — Vehicle | 2076A KO — Vehicle | 2076A

B

WT — Vehicle | 2076A KO — Vehicle | 2076A

C

Liver weight (g): WT, KO (Vehicle vs 2076A); *

Liver weight/body weight %: WT, KO (Vehicle vs 2076A)

D

TG content in liver (ug/mg protein): WT, KO; **

E

Total cholesterol content in liver (ug/mg protein): WT, KO; **

F

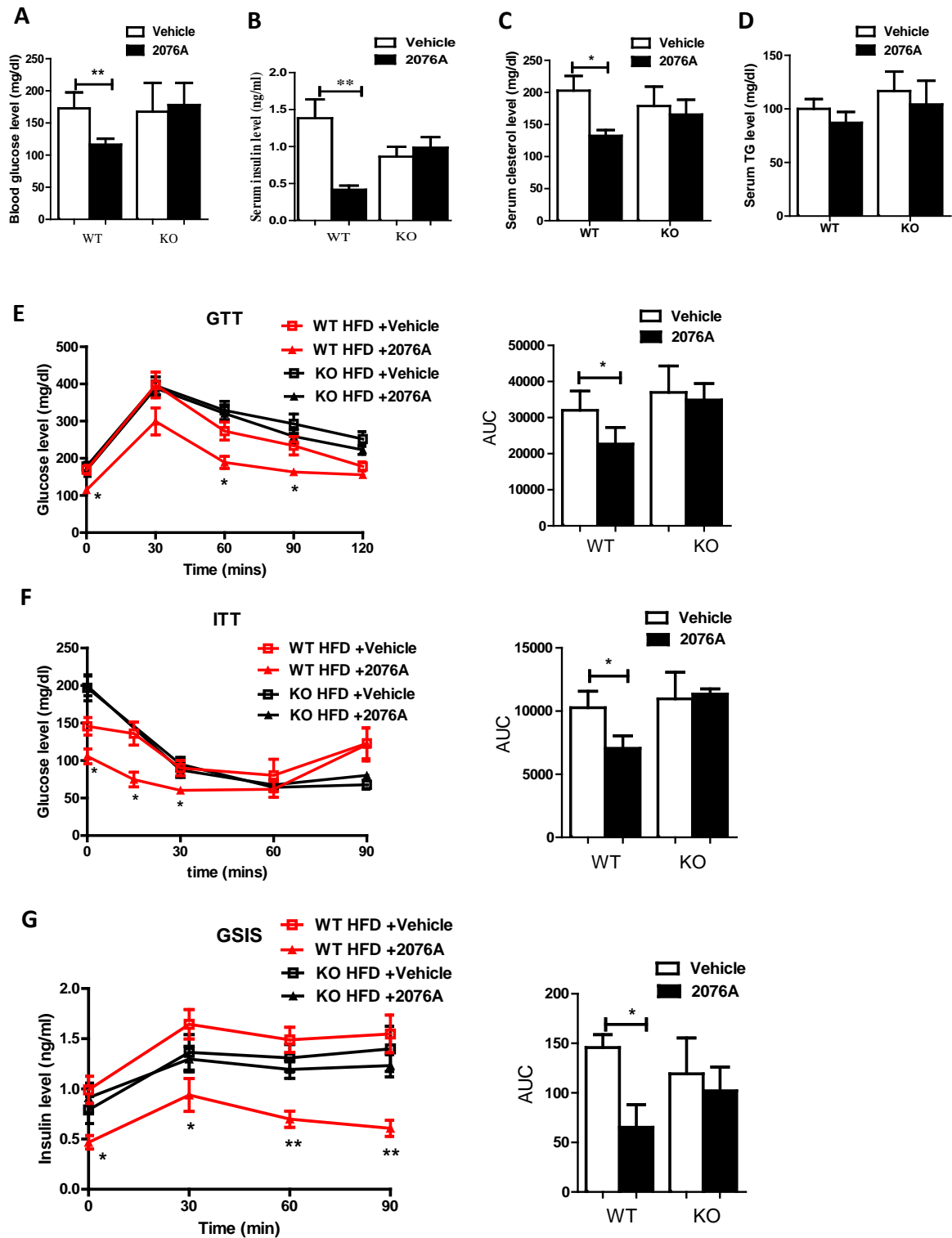Relative mRNA levels: MACD, ACC, FAS, SREBP, L-FABP (WT vs KO; Vehicle vs 2076A); *, *, *, *, **

Figure 6

Figure 7